DLTFS investigation of electron traps on AlGaN/GaN on Si Power diodes

Florian Rigaud-Minet, Christophe Raynaud, Julien Buckley, Matthew Charles, Patricia Pimenta-Barros, Romain Gwoziecki, Charlotte Gillot, Véronique Sousa, Hervé Morel, Dominique Planson

energies

MDPI

Article

Deep Level Transient Fourier Spectroscopy Investigation of Electron Traps on AlGaN/GaN-on-Si Power Diodes

Florian Rigaud-Minet [1,2,*], Christophe Raynaud [1,*], Julien Buckley [2], Matthew Charles [2], Patricia Pimenta-Barros [2], Romain Gwoziecki [2], Charlotte Gillot [2], Véronique Sousa [2], Hervé Morel [1] and Dominique Planson [1]

[1] Univ Lyon, INSA Lyon, Université Claude Bernard Lyon 1, Ecole Centrale de Lyon, CNRS, Ampère, UMR5005, F-69621 Villeurbanne, France
[2] Univ. Grenoble Alpes, CEA, Leti, F-38000 Grenoble, France
* Correspondence: florian.rigaud-minet@cea.fr (F.R.-M.); christophe.raynaud@insa-lyon.fr (C.R.)

Abstract: Many kinds of defects are present in AlGaN/GaN-on-Si based power electronics devices. Their identification is the first step to understand and improve device performance. Electron traps are investigated in AlGaN/GaN-on-Si power diodes using deep level transient Fourier spectroscopy (DLTFS) at different bias conditions for two Schottky contact's etching recipes. This study reveals seven different traps corresponding to point defects. Their energy level E_T ranged from 0.4 eV to 0.57 eV below the conduction band. Among them, two new traps are reported and are etching-related: D3 (E_T = 0.47–0.48 eV; $\sigma \approx 10^{-15}$ cm^2) and D7 (E_T = 0.57 eV; $\sigma = 4.45 \times 10^{-12}$ cm^2). The possible origin of the other traps are discussed with respect to the GaN literature. They are proposed to be related to carbon and nitrogen vacancies or to carbon, such as C_N-C_{Ga}. Some others are likely due to crystal surface recombination, native defects or a related complex, or to the nitrogen antisite: N_{Ga}.

Keywords: power electronics; wide bandgap; gallium nitride; DLTS; reactive ion etching; traps

Citation: Rigaud-Minet, F.; Raynaud, C.; Buckley, J.; Charles, M.; Pimenta-Barros, P.; Gwoziecki, R.; Gillot, C.; Sousa, V.; Morel, H.; Planson, D. Deep Level Transient Fourier Spectroscopy Investigation of Electron Traps on AlGaN/GaN-on-Si Power Diodes. *Energies* **2023**, *16*, 599. https://doi.org/10.3390/en16020599

Academic Editor: Gianluca Brando

Received: 5 December 2022
Revised: 23 December 2022
Accepted: 27 December 2022
Published: 4 January 2023

1. Introduction

The AlGaN/GaN heterostructure is attractive for making power devices such as Schottky barrier diodes (SBD) and normally-off heterostructure field effect transistors for medium voltage (100 V–1000 V) [1] and high frequency applications [2,3]. This is achievable because of the transport properties in the two-dimensional electron gas (2DEG) [4] and high breakdown field of 3.3 MV/cm of bulk GaN [5]. However, the presence of traps either restricts the performance of the device, as demonstrated for the leakage current of diodes [6], or at least degrades its electrical characteristics, as in the case of current collapse [7,8].

One of the best-adapted techniques for trap identification is deep level transient spectroscopy (DLTS). With this technique, unintentionally doped and n-GaN samples fabricated using an inductively coupled plasma-reactive induced etching (ICP-RIE) step were investigated [9–12]. Traps related to nitrogen vacancies were found: V_N at E_T = 0.23 to 0.25 eV below the conduction band [10,11] and traps near the surface of the epitaxial layers [12]. AlGaN/GaN devices were also studied [12–21]. Traps related to native defects were found [13] in addition to interface traps [14,15], buffer traps [14] and etching-related traps [12,20]. The distinction between the GaN buffer and the AlGaN barrier location in diodes was unclear [16], while applying polarization to a non-recessed high electron mobility transistor gave another degree of freedom to clarify this [17].

In this study, the presence of electron traps in two 650 V/6 A AlGaN/GaN-on-Si fully-recessed SBDs having different ICP-RIE recipes for the Schottky contact formation was investigated by DLTFS measurements. Indeed, the recipes were found to affect the current characteristics. The obtained traps spectra are analyzed and discussed with respect to the traps reported in the literature.

2. Materials and Methods

The device used in this study is a 650 V/6 A AlGaN/GaN fully-recessed Schottky barrier diode fabricated at CEA LETI. It was manufactured on 3.5 µm of epitaxial layers grown by metal organic vapor phase epitaxy (MOVPE) in an AIXTRON® G5+® tool (AIXTRON SE, Herzogenrath, Germany). The epitaxial structure was composed of six different parts (Figure 1a): an AlN nucleation layer, $Al_xGa_{1-x}N$ Strain Relief Layers (SRL), a thick GaN:C layer, active unintentionally doped (UID) GaN/AlN/AlGaN layers (similar to [22]), and finally, an in situ Si_3N_4 layer to protect the heterojunction. They were grown on a 1 mm thick, 200 mm diameter (111)-silicon substrates with a resistivity between 3 and 20 Ω.cm. On top of the structure, Si_3N_4 and SiO_2 passivation layers were deposited. The ohmic contacts were obtained by etching the passivation and barrier layers directly in contact with the 2DEG, then depositing a Ti/Al bilayer. Later, the anode recess was created by etching the passivation layers and the $Al_xGa_{1-x}N$, using ICP-RIE with BCl_3/Cl_2 as the reactive gases for the $Al_xGa_{1-x}N$ etch. The two etching conditions studied here, named LV 90 V and LV 237 V, are summarized in Table 1. A dry photoresist stripping was performed with O_2/N_2 plasma. After that, a wet clean with EKC265 (DuPont® EKC Technology, Hayward, CA, United-States) was applied followed by rinsing. Subsequently, titanium nitride (TiN) and tungsten (W) were successively deposited before some back end of line steps to form electrical contact pads.

The characterized device is an inter-digitated comb-like diode with a 60 mm width, with the cross-section illustrated in Figure 1a. The distance between the anode and the cathode (L_{AC}) is 16 µm, the anode field plates: (FPG0 to FPG3) are 1 µm long, and the cathode field plate (FPD) is 0.5 µm. Figure 1b,c show scanning transmission electron microscopy (STEM) in high-angle annular dark field (HAADF). These observations confirm that there is no significant difference in the etching morphology between the two devices.

However, as it can be observed in Figure 2a,b, the electrical characteristics (forward and reverse current, respectively) of the Schottky diode are influenced by the etching recipe.

Table 1. ICP-RIE etching split table.

Experimental Split	ICP Source (W)	RF Bias (V)	BCl_3/Cl_2 Ratio
LV 90 V	500	90	1
LV 237 V	300	237	4

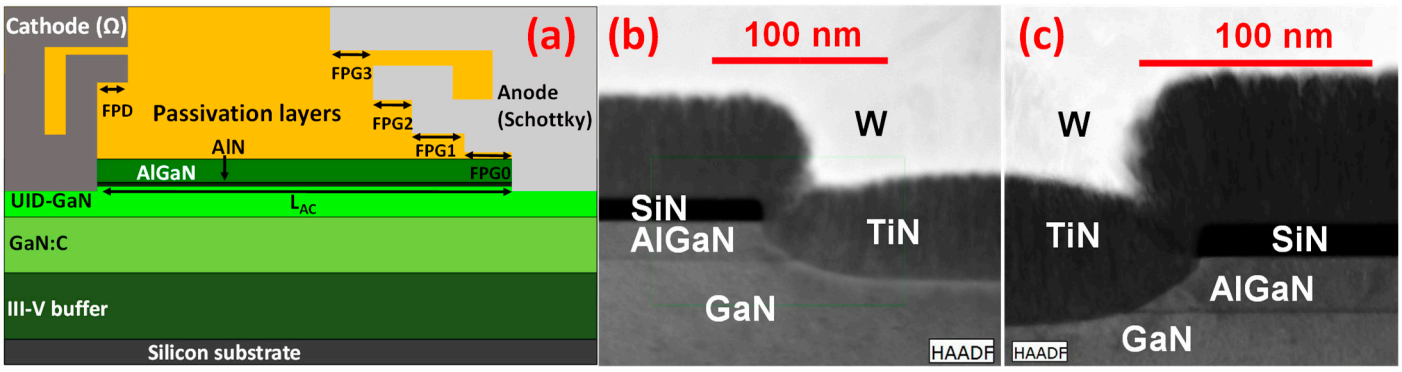

Figure 1. (**a**) Detailed cross-section of the structure; (**b**) STEM observation of the LV 90 V Schottky interface; (**c**) STEM observation of the LV 237 V Schottky interface.

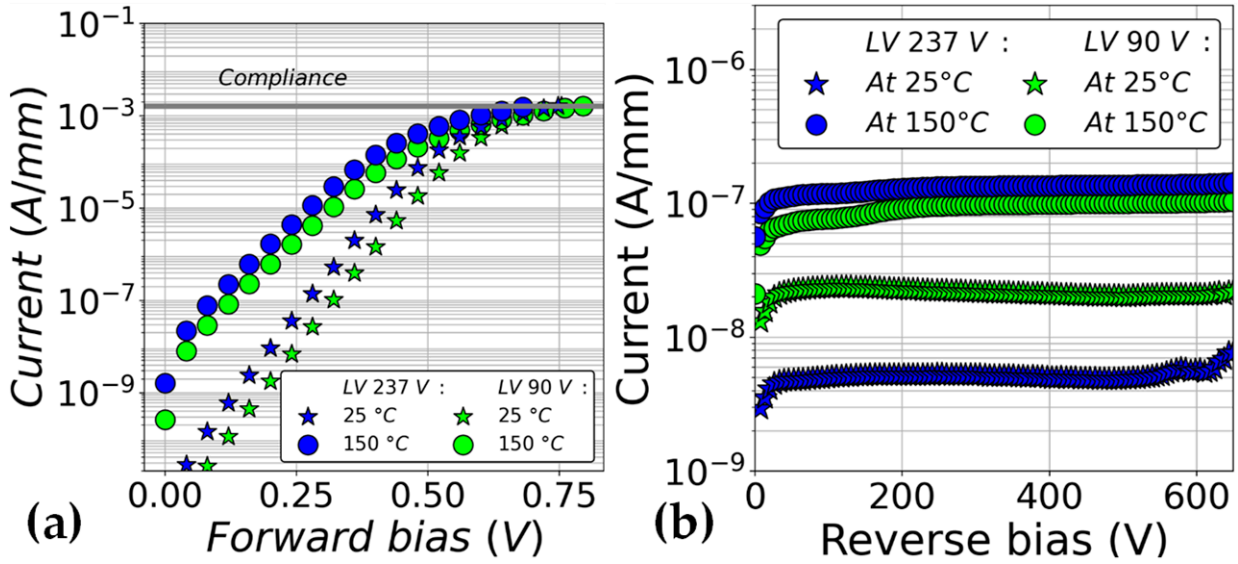

Figure 2. (**a**) Typical low voltage forward characteristics; (**b**) Typical reverse characteristics of the two experimental splits.

For the forward regime, it can be seen in Figure 2a that the LV 237 V characteristic is slightly shifted to the left with respect to the LV 90 V. This was explained by a small decrease in the barrier height (from 0.68 ± 0.01 to 0.64 ± 0.04), revealed by a temperature dependency analysis (not shown here). In addition, the ideality factor of the diode (defined in [23]) are very similar (=1.16 ± 0.05) in both experimental splits.

The leakage current temperature dependence in the reverse regime is also changed with the etching conditions. Indeed, the leakage values are similar at 150 °C, whereas at 25 °C, the leakage is reduced for the LV 237 V split.

These changes may be due to the traps that will be probed in this article by DLTFS.

The experimental splits were tested on a DLTS test setup: FT-1030 HERA-DLTS® (High energy resolution analysis deep level transient spectroscopy) system (PhysTech® GmbH, Moosburg an der Isar, Germany) [24,25]. Measurements were performed from 50 K to 425 K and, in this article, only capacitance DLTFS (C-DLTFS) results measured with a Boonton 7200 capacitance meter are presented. Samples were kept in the dark during all of the experiments. The first order Fourier sine (resp. cos) coefficient b1 (resp. a1) [24,26] were chosen to represent the DLTFS signal.

3. Results

For this study, the DLTFS spectrum was recorded for both samples at different reverse biases: −10 V; −20 V; −50 V; −70 V and −90 V, to probe different regions of the heterojunction device. An example of the obtained spectra is shown in Figure 3. This was obtained with a positive voltage bias: V_P equal to 0 V or −0.1 V, a reverse bias V_R equal to −50 V, a filling pulse time: t_P of 100 µs, and a time window: T_W equal to 2.048 ms. On this graph, two peaks can be seen: E_1 and E_2, and correspond to two different kinds of traps.

For all of the chosen biases and the different samples, Arrhenius plots were calculated and trap properties were extracted, as illustrated in Figure 4. The trap energy level E_T and the electron trap capture cross-section: σ_{e^-} have been extracted from the Arrhenius plot using the following formula [27]:

$$\frac{e_n}{T^2} = \frac{4\sqrt{6}\pi^{\frac{3}{2}} m^*_{e^-} K_B{}^2 \sigma_{e^-}}{h^3} \exp\left(\frac{-E_T}{K_B T}\right) \quad (1)$$

The parameter e_n is the electron emission rate, T is the temperature, K_B is the Boltzmann constant, h is the Planck constant and $m^*_{e^-}$ is the electron effective mass equal to $0.2 \times m_0$ [28]. Note that E_T is measured from the conduction band.

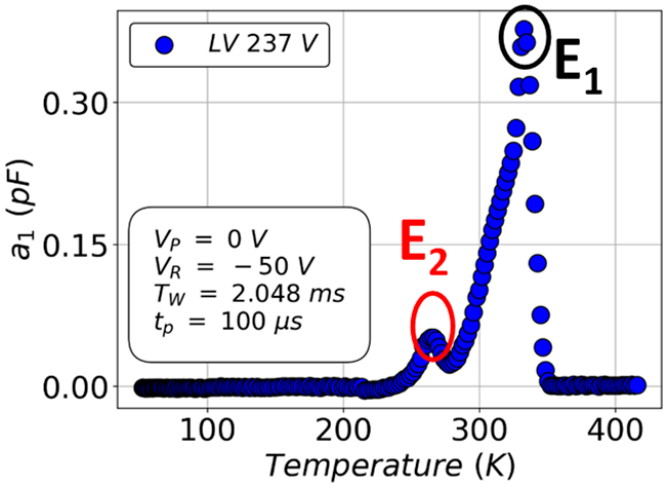

Figure 3. A typical DLTFS temperature scan of the LV 237 V diode recorded at $V_R = -50$ V; $V_P = 0.0$ V; $t_P = 100$ µs, and $T_W = 2.048$ ms.

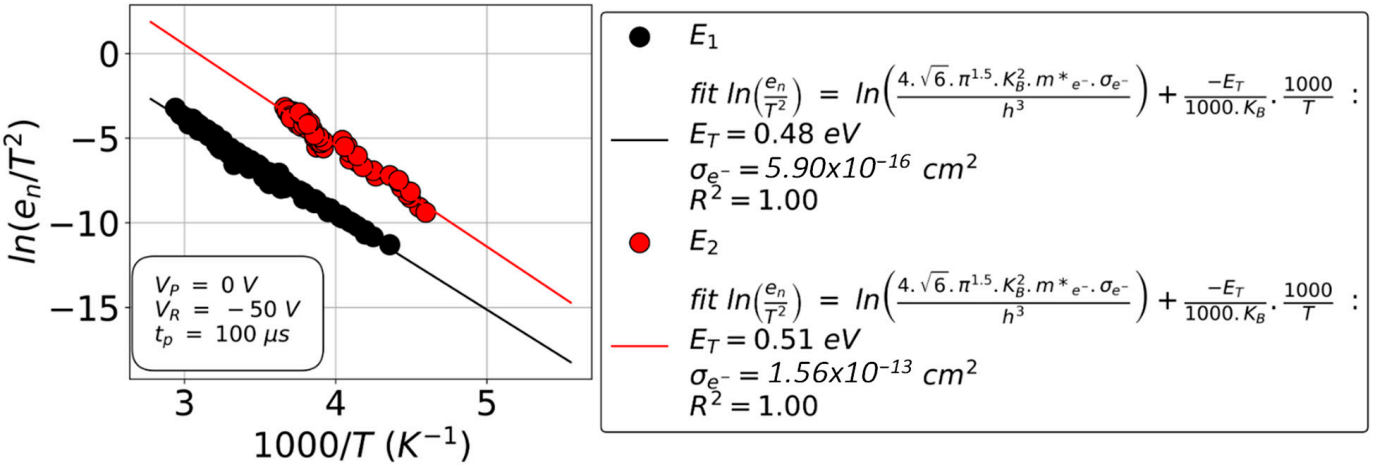

Figure 4. DLTFS Arrhenius plot of the LV 237 V diode recorded at $V_R = -50$ V; $V_P = 0$ V and $t_P = 100$ µs.

From Figure 4, the trap properties of the two peaks identified in Figure 3 can be extracted. The peak E_1, which has the maximum amplitude in Figure 3, corresponds to an electron trap with an energy level at 0.48 eV below the conduction band and a cross-section σ_{e^-} of 5.9×10^{-16} cm^2, whereas the second peak E_2 is related to an energy level $E_C - E_T = 0.51$ eV with $\sigma_{e^-} = 1.56 \times 10^{-13}$ cm^2.

This analysis was conducted for all of the voltage biases and for both samples except for the sample LV 237 V at −90 V bias. Two peaks overlapped, which required the use of high energy resolution analysis by Laplace and deconvolution using a Provencher's CONTIN algorithm [29,30] to distinguish one peak from the other.

The data extracted from the measurements are summarized in Table 2. In this table, the different traps reported are gathered in different groups, named D_i with $i \in [|1,7|]$. The groups were constructed by gathering traps that have similar properties: energy level (range not exceeding 20 meV) and cross-section (range within one and a half decades). It must be known that the range values are empirical but the different groups were confirmed especially with their qualitative common Fourier coefficient dependency as a function of the filling pulse time (t_P).

Table 2. Energies and cross-sections extracted from Arrhenius plots for the different samples and at different bias conditions gathered in category D_i, with the proposed hypothesis for each category.

		D1		D2		D3		D4		D5		D6		D7	
		E_T (eV)	σ (cm^2)	E_T (eV)	σ (cm^2)	E_T (eV)	σ (cm^2)	E_T (eV)	σ (cm^2)	E_T (eV)	σ (cm^2)	E_T (eV)	σ (cm^2)	E_T (eV)	σ (cm^2)
U_P = −0.1 V U_R = −10 V	LV 237 V									0.53	1.55×10^{-13}				
	LV 90 V													0.57	4.45×10^{-12}
U_P = −0.1 V U_R = −20 V	LV 237 V							0.50	1.73×10^{-13}						
	LV 90 V							0.49	7.58×10^{-15}	0.54	2.85×10^{-13}				
U_P = 0 V U_R = −50 V	LV 237 V					0.48	5.90×10^{-16}	0.51	1.56×10^{-13}						
	LV 90 V			0.46	2.56×10^{-13}					0.52	1.49×10^{-14}				
U_P = 0 V U_R = −70 V	LV 237 V					0.47	7.14×10^{-16}					0.55	4.33×10^{-15}		
	LV 90 V											0.55	1.39×10^{-14}		
U_P = 0 V U_R = −90 V	LV 237 V	0.40	7.98×10^{-18}			0.47	1.13×10^{-15}					0.55	4.21×10^{-15}		
	LV 90 V											0.56	1.59×10^{-14}		
Proposed Hypothesis		C_{Ga}-V_N		Surface recombination		Etching-related		Native defects or related complex		C_N-C_{Ga}		N_{Ga}		Etching-related	

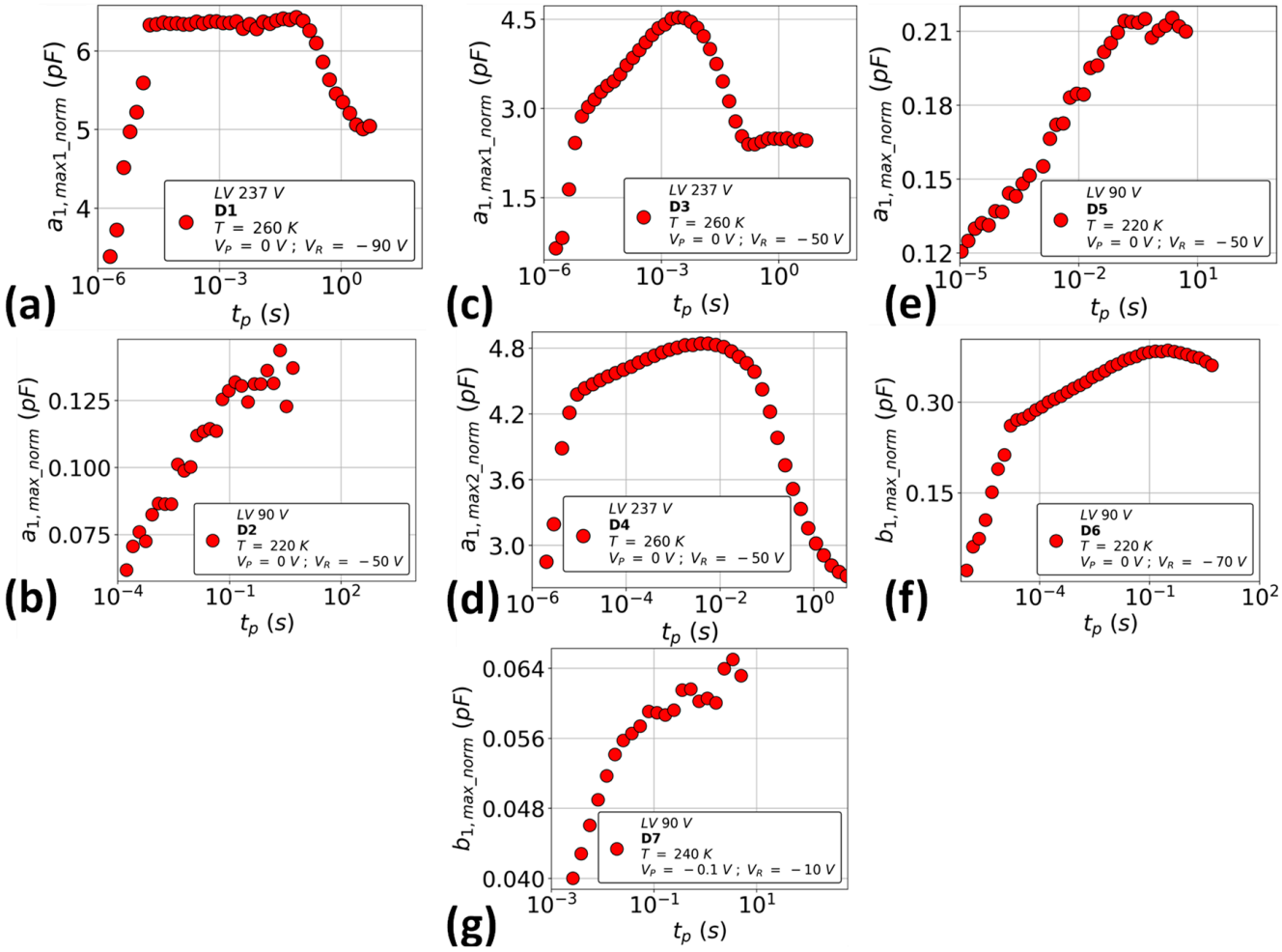

Figure 5. DLTFS normalized peak amplitude versus the filling pulse width: t_p for the trap levels observed in both samples (**a**) D1; (**b**) D2; (**c**) D3; (**d**) D4; (**e**) D5; (**f**) D6; (**g**) D7. Note: Some signals are not available for the entire t_P range because the peaks were out of the measured range or were too small.

The signature of every trap group as a function of the filling pulse time (t_P) is shown in Figure 5. The signatures were represented independently of the chosen coefficient (b1 or a1), since both give the same signature for a given trap. All traps correspond to point defects, since their characteristics are not entirely linear in the whole t_P range as should be the case for an extended defect, such as dislocation [31]. The observed trends can be separated into two different categories. Category A is constituted of D1, D2 and D5 because their peak amplitude is proportional to the filling pulse width logarithm in a single part of the plot, as shown in Figure 5a,b,e. This trend has already been observed in the literature [32,33]. Category B is characterized by a linear increase, with the logarithm of the filling pulse width along two subsequent slopes, as for D3, D4, D6 and D7 (Figure 5c,d,f,g). A decrease in the DLTFS peak amplitude signal at high pulse width can be observed for Groups D1, D3, D4 and D6. This was already reported in the study by Soh et al. [33] and would correspond to an emission process in the main capturing section. It must be understood that the emission section is analysed in DLTS (as explained with Equation (1)); thus, the hypothesis of a capture process within the emission section is more coherent. According to the same author, the linear increase with the logarithm of the filling pulse width in a given part of the signature involves the proximity of the point defects with a dislocation. Polenta et al. in [34] agrees with this assertion, however, the consensus is not currently established, thus requiring further investigation.

4. Discussion

Having grouped the electron traps by energy levels and cross-sections, they could be compared with the reported traps between 0.36 eV and 0.61 eV in the experimental literature [9,12–14,16–20,27,32–52], as shown in Figure 6, and with the theoretical study made by Jenkins et al. [53] and Gorczyca et al. [54], but also with trap energy levels that were not reported with cross-sections. The trap presence at a specific bias or voltage range is not included in the discussion, since a peak related to a given trap can be hidden by another.

Firstly, Group D1 corresponds to an energy of 0.40 eV and a cross-section of 7.98×10^{-18} cm^2. In Figure 6, the nearest traps were reported in [19,33]. However, the trap reported in [33], was present only in silicon doped samples, so the author suggested that the trap was due to Si_{Ga}. Since no silicon is present in the studied samples, this hypothesis is thus put aside. The C-related hypothesis of [19] comes from the ab-initio computations of Matsubara et al. [55]. The C_{Ga}-V_N was found to have the (3+/2+) thermodynamic transition at 0.40 eV. This hypothesis is coherent with the point nature of the defect shown in Figure 5a as well as finding them in Pd/Au [33] and TiN (studied samples) Schottky contacts. In addition, it was only found in the LV 237 V, which has a higher RF bias during etching than LV 90 V, and this increased RF bias is likely to create more nitrogen vacancies [56]. By contrast, Tanaka et al. in [57] and Arehart et al. [58] found a trap at 0.4 eV (without a reported cross-section). This energy level was present in GaN-on-SiC samples but not in GaN-on-GaN, leading to a trap hypothesis of a crystal mismatch defect [57], and was present in ammonia-molecular beam epitaxy grown samples with a high NH_3/Ga flux ratio [58]. By assuming that a high NH_3/Ga flux leads to a lower concentration of nitrogen vacancies, this means that the traps reported may be different from the ones reported in this study. These reported traps (with an unknown cross-section) could be associated with higher cross-section traps; however, having the same energy in Figure 6 as reported by Honda et al. in [42] (C-related trap), Ferrandis et al. [12] (damage induced defect), and Polyakov et al. [17] (bulk defect). This would mean that Group D1 can be related to C_{Ga}-V_N, whereas traps with a higher cross-section may have a different physical origin.

Group D2 is placed in the vicinity of the trap reported by [17,40,45,46] in Figure 6 and has the same energy level of traps reported in [15,50,59]. This trap level is present only for titanium based contacts, not for the tantalum or indium based ones in Boturchuk et al. [40], and for nickel and gold based contacts [17,45,46], which means that the trap is located near the surface but not related to surface contamination. This is further confirmed with the increase in its concentration after electron or neutron bombardment [15,46], and its disappearance with proton irradiation [45]. The bias dependent experiment of Polyakov et al. [17], performed on a lateral transistor, and the presence in n-GaN samples suggest that the point defect is not device specific. No additional comments can be made with the presence or not of a 0.45 eV defect in AlGaN/GaN superlattice as reported in [50], since there is no cross-section evaluation. It can be noted that it is only present in the LV 90 V sample, which means that the etching conditions play a role in its presence. The most probable hypothesis following the previous statements would be surface recombination.

As for Group D3, it is reported only in the LV 237 V sample. Thus, it is related to the etched surface, similarly to D2, but enhanced in different etching conditions. Its novelty is proven by the distance of its properties, which are far from the other points in Figure 6. Further study, separating the different etching parameters, could be performed to further investigate its origin.

Groups D4 and D5 have similar cross-sections that present a high dispersion. It is important to remember that the grouping was confirmed with the trap filling pulse width signature (not shown here). However, this specific shape has not been investigated in the present study. It could be the subject of a future study.

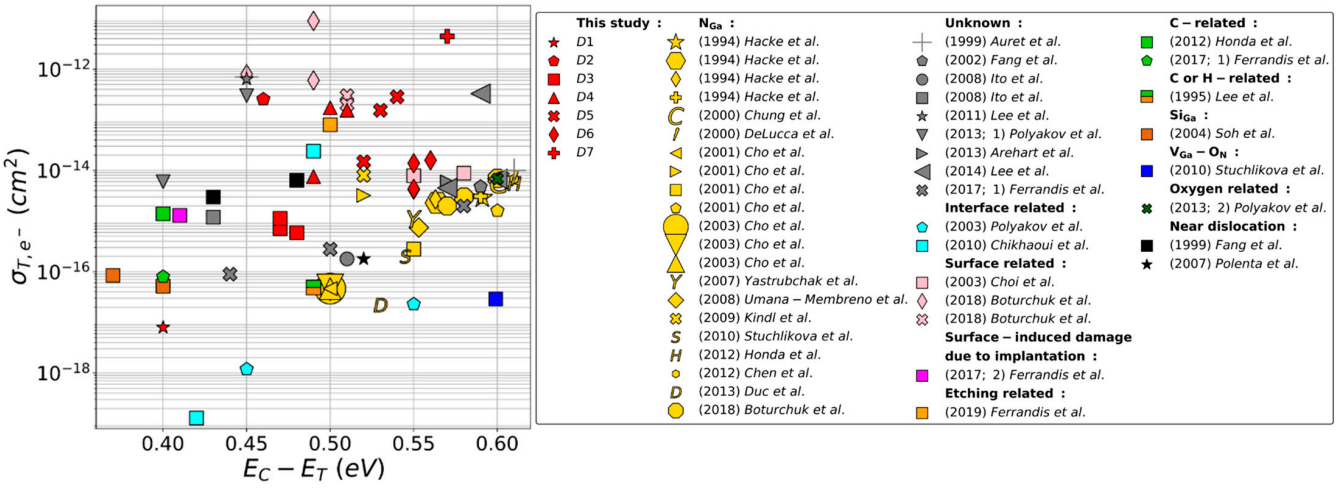

Figure 6. Extracted cross-section as a function of the trap energy from DLTS measurements from this study and the literature corresponding to point defects with an energy level between 0.36 eV and 0.61 eV (Authors references: (1994) Hacke et al. [37]; (1995) Lee et al. [51]; (1999) Auret et al. [45]; (1999) Fang et al. [52]; (2000) Chung et al. [41]; (2000) Delucca et al. [44]; (2001) Cho et al. [36]; (2002) Fang et al. [48]; (2003) Cho et al. [35]; (2003) Choi et al. [9]; (2003) Polyakov et al. [50]; (2004) Soh et al. [33]; (2007) Yastrubchak et al. [32]; (2007) Polenta et al. [34]; (2008) Umana-Membreno et al. [38]; (2008) Ito et al. [47]; (2009) Kindl et al. [27]; (2010) Stuchlikova et al. [13]; (2010) Chikhaoui et al. [14]; (2011) Lee et al. [46]; (2012) Honda et al. [42]; (2012) Chen et al. [43]; (2013) Duc et al. [39]; (2013; 1) Polyakov et al. [17]; (2013) Arehart et al. [16]; (2013; 2) Polyakov et al. [18]; (2014) Lee et al. [49]; (2017; 1) Ferrandis et al. [19]; (2017; 2) Ferrandis et al. [12]; (2018) Boturchuk et al. [40]; (2019) Ferrandis et al. [20]).

Focusing our attention on D4, these values are close to the traps reported in [14,20,40,52] in Figure 6. They depend neither on the growth technique, because a reactive molecular beam epitaxy is used in [52] and metal organic chemical vapor deposition in [14,20,40], nor on Schottky contact, because it was observed in molybdenum and gold [14], gold [40] based Schottky contact, and also in metal oxide semiconductor high electron mobility [20]. The etching-related trap hypothesis by Ferrandis et al. [20] can be rejected in the present study because the trap is present in samples that were not etched [52]. The extended defect hypothesis of [40] can be rejected in the present study as well, since the filling pulse width dependence has not been provided. A 0.49 eV energy level reported by Götz et al. in [60] could have brought further information if cross-sections were extracted. In addition, the presence of these traps in both of the studied samples does not give additional information. Thus, despite the lack of clues on their origin, these traps correspond either to native defects or related complexes since they neither depend on the growth technique nor on the deposited Schottky metal.

Focusing our attention now on Group D5, especially on the point of this group that has the smallest reported cross-section in Figure 6, it is close to two reported traps in the literature [27,36]. The hypothesis proposed by those authors can be questioned since, for instance, the comparison of trap energy levels of 0.52 ± 0.01 eV in [27] with 0.598 ± 0.01 eV traps in [61] is inaccurate. However, traps were reported in MOVPE [27,36] with very specific growth conditions (Trimethylgallium (TMGa) flux and growth rate) [36]. Moreover, the ab-initio computations of Matsubara et al. [55] revealed that the (+/0) thermodynamic transition of C_N-C_{Ga} is located at 0.52 eV. The presence of carbon in the epitaxy due to the methyl group present in the precursor TMGa is coherent with this hypothesis. Furthermore, this is coherent with its presence in samples having a different Schottky contact metal (titanium or aluminum [27], and gold [36]). Thus, D5 could be related to C_N-C_{Ga}.

As for Group D6, they are tightly grouped together in Figure 6 and found near the trap reported in [9], and the traps reported at a slightly higher energy [16,49]. A comparison cannot be performed with the lower cross-section reported in the study of Yastrubchak et al.

in [32] since they do not have the same filling pulse width dependence. In addition, a trap level at 0.55 eV was reported to increase with the electron bombardment in the study of Hwang et al. [15]; however, the lack of a reported cross-section prevents the comparison with Group D6. To begin with, the discussion on the origin of this group, Choi et al. [9], states that the defect level is unrelated to the etching. This is coherent with the fact that it is detected in both of the studied samples here. Moreover, it is present in samples having a platinum ([9]) and TiN (studied samples) based Schottky contact, which puts the surface contaminant hypothesis aside. In addition, it is present in an as-grown GaN sample, meaning that the hypothesis of a trap in the AlGaN barrier or at the AlGaN/passivation interface can be discarded in the present study. Nevertheless, the hypothesis of native GaN defects is coherent with its presence in an n-GaN [9] system and an AlGaN/GaN system [16,49,50]. The theoretical study of Jenkins et al. [53] and Gorczyca et al. [54] calculates the position (energy level) associated with nitrogen on the Ga-site (antisite): N_{Ga} in the band gap. The most recent study [54], based on ab-initio calculations using a supercell approach in connection with the full potential-linear muffin-tin orbital method, reports an energy of 0.55 eV for N_{Ga}, which perfectly corresponds to the level found in both studied samples. This is, therefore, the chosen hypothesis for Group D6. It must be noted that many authors used this as a hypothesis, as it can be seen in Figure 6.

Finally, Group D7 has no reported traps in its vicinity in Figure 6. It was detected only in the sample LV 90 V, meaning that it is related to the etching conditions. Further studies, with a variation in individual etching parameters, could be performed to understand the origin of the observed difference.

To conclude the discussion on other spectroscopies that could confirm the findings, current collapse measurements were performed on the same kind of Schottky diode in the article of Lorin et al. [22]. Group D1 and D6 were potentially also detected (the uncertainty lies in the lack of extracted cross-sections), which is coherent with our findings. The difference in the traps found (present in one study and not in the other) lies in the voltage stress difference that would change the probed area and traps' concentration. Furthermore, optical-DLTS could not have been performed on the studied sample because the metallic field plate would have screened the optical beam near the Schottky contact region.

5. Conclusions

In this study, the electron traps of two 650 V/6 A fully-recessed AlGaN/GaN-on-Si Schottky barrier diodes having two different Schottky contact etching recipes were studied. Indeed, the current characteristics in the forward and reverse regimes are significantly changed in contrast with the contact morphology. This study was performed using C-DLTFS and HERA-DLTFS techniques between 50 K to 425 K and by biasing the device between a positive bias of 0 V and a reverse bias ranging from −10 V to −90 V. Seven different trap groups were gathered according to their similar energy level, and the cross-section and filling pulse width dependence were reported. Their energies' E_T range lay between 0.4 eV and 0.57 eV, and since no linear dependence as a function of the filling pulse width logarithm was observed across their entire range, they were associated with point defects.

By making an exhaustive comparison with the GaN trap literature, new traps were reported to be etching-related: D3 (E_T = 0.47–0.48 eV; $\sigma \approx 10^{-15}$ cm^2) due to its unique presence in the LV 237 V sample, and D7 (E_T = 0.57 eV; $\sigma = 4.45 \times 10^{-12}$ cm^2) due to its unique presence in the LV 90 V sample. Concerning the other traps, Group D1 was proposed to be related to carbon and nitrogen vacancies. Group D2 is likely to be a surface crystal recombination trap. As for Group D4, it is probably related to native defects or related complexes. Concerning Group D5, it is perhaps related to carbon with a C_N-C_{Ga} hypothesis suggested by comparison with theoretical calculations from the literature, and finally, Group D6 could be related to the nitrogen antisite, N_{Ga}.

Author Contributions: Conceptualization, F.R.-M.; Data curation, F.R.-M. and C.R.; Formal analysis, F.R.-M.; Investigation, F.R.-M.; Methodology, F.R.-M.; Project administration, R.G., C.G. and V.S.; Resources, C.R., M.C. and P.P.-B.; Supervision, C.R., J.B., V.S., H.M. and D.P.; Validation, C.R.; Writing—

original draft, F.R.-M.; Writing—review and editing, F.R.-M., C.R., J.B., M.C., P.P.-B., R.G., C.G., V.S., H.M. and D.P. All authors have read and agreed to the published version of the manuscript.

Funding: This work was partially supported by the French Public Authorities within the frame of the PSPC French national program «G-Mobility».

Data Availability Statement: Data is contained within the article.

Conflicts of Interest: The authors declare no conflict of interest.

References

1. Meneghini, M.; De Santi, C.; Abid, I.; Buffolo, M.; Cioni, M.; Khadar, R.A.; Nela, L.; Zagni, N.; Chini, A.; Medjdoub, F.; et al. GaN-Based Power Devices: Physics, Reliability, and Perspectives. *J. Appl. Phys.* **2021**, *130*, 181101. [CrossRef]
2. Di Paolo Emilio, M. Markets Turn to Wide-Bandgap Semiconductors to Increase Power Efficiency. *EE Times Eur.* **2020**. Available online: https://www.eetimes.eu/markets-turn-to-wide-bandgap-semiconductors-to-increase-power-efficiency/2/ (accessed on 29 December 2022).
3. Zhao, X.; Yeh, C.-S.; Chen, C.-W.; Lai, J.-S. A Comprehensive Comparison of MHz GaN-Based ZVS Step-Down Converters for Low Power Integrated On-Chip Applications. In Proceedings of the 2018 IEEE Energy Conversion Congress and Exposition (ECCE), Portland, OR, USA, 23–27 September 2018; pp. 5271–5275. [CrossRef]
4. Mohammad, S.N.; Salvador, A.A.; Morkoc, H. Emerging Gallium Nitride Based Devices. *Proc. IEEE* **1995**, *83*, 1306–1355. [CrossRef]
5. Gaskill, D.K.; Brandt, C.D.; Nemanich, R.J. (Eds.) *III-Nitride, SiC, and Diamond Materials for Electronic Devices, San Francisco, CA, USA, 8–12 April 1996*; Materials Research Society: Pittsburgh, PA, USA, 1996; ISBN 978-1-55899-326-6.
6. Soni, A.; Shikha, S.; Shrivastava, M. On the Role of Interface States in AlGaN/GaN Schottky Recessed Diodes: Physical Insights, Performance Tradeoff, and Engineering Guidelines. *IEEE Trans. Electron Devices* **2019**, *66*, 2569–2576. [CrossRef]
7. Uren, M.J.; Silvestri, M.; Casar, M.; Hurkx, G.A.M.; Croon, J.A.; Sonsky, J.; Kuball, M. Intentionally Carbon-Doped AlGaN/GaN HEMTs: Necessity for Vertical Leakage Paths. *IEEE Electron Device Lett.* **2014**, *35*, 327–329. [CrossRef]
8. Wach, F.; Uren, M.J.; Bakeroot, B.; Zhao, M.; Decoutere, S.; Kuball, M. Low Field Vertical Charge Transport in the Channel and Buffer Layers of GaN-on-Si High Electron Mobility Transistors. *IEEE Electron Device Lett.* **2020**, *41*, 1754–1757. [CrossRef]
9. Choi, K.J.; Jang, H.W.; Lee, J.-L. Observation of Inductively Coupled-Plasma-Induced Damage on n-Type GaN Using Deep-Level Transient Spectroscopy. *Appl. Phys. Lett.* **2003**, *82*, 1233–1235. [CrossRef]
10. Fang, Z.-Q.; Look, D.C.; Wang, X.-L.; Han, J.; Khan, F.A.; Adesida, I. Plasma-Etching-Enhanced Deep Centers in n-GaN Grown by Metalorganic Chemical-Vapor Deposition. *Appl. Phys. Lett.* **2003**, *82*, 1562–1564. [CrossRef]
11. Cho, H.K.; Khan, F.A.; Adesida, I.; Fang, Z.-Q.; Look, D.C. Deep Level Characteristics in N-GaN with Inductively Coupled Plasma Damage. *J. Phys. D Appl. Phys.* **2008**, *41*, 155314. [CrossRef]
12. Ferrandis, P.; Charles, M.; Baines, Y.; Buckley, J.; Garnier, G.; Gillot, C.; Reimbold, G. Ion-Assisted Gate Recess Process Induced Damage in GaN Channel of AlGaN/GaN Schottky Barrier Diodes Studied by Deep Level Transient Spectroscopy. *Jpn. J. Appl. Phys.* **2017**, *56*, 04CG01. [CrossRef]
13. Stuchlikova, L.; Sebok, J.; Rybar, J.; Petrus, M.; Nemec, M.; Harmatha, L.; Benkovska, J.; Kovac, J.; Skriniarova, J.; Lalinsky, T.; et al. Investigation of Deep Energy Levels in Heterostructures Based on GaN by DLTS. In Proceedings of the 8th International Conference on Advanced Semiconductor Devices & Microsystems (ASDAM), Smolenice Castle, Slovakia, 25–27 October 2010; pp. 135–138. [CrossRef]
14. Chikhaoui, W.; Bluet, J.M.; Bru-Chevallier, C.; Dua, C.; Aubry, R. Deep Traps Analysis in AlGaN/GaN Heterostructure Transistors. *Phys. Status Solidi (C)* **2010**, *7*, 92–95. [CrossRef]
15. Hwang, Y.-S.; Liu, L.; Ren, F.; Polyakov, A.Y.; Smirnov, N.B.; Govorkov, A.V.; Kozhukhova, E.A.; Kolin, N.G.; Boiko, V.M.; Vereyovkin, S.S.; et al. Effect of Electron Irradiation on AlGaN/GaN and InAlN/GaN Heterojunctions. *J. Vac. Sci. Technol. B Nanotechnol. Microelectron. Mater. Process. Meas. Phenom.* **2013**, *31*, 22206. [CrossRef]
16. Arehart, A.R.; Sasikumar, A.; Rajan, S.; Via, G.D.; Poling, B.; Winningham, B.; Heller, E.R.; Brown, D.; Pei, Y.; Recht, F.; et al. Direct Observation of 0.57eV Trap-Related RF Output Power Reduction in AlGaN/GaN High Electron Mobility Transistors. *Solid-State Electron.* **2013**, *80*, 19–22. [CrossRef]
17. Polyakov, A.Y.; Smirnov, N.B.; Govorkov, A.V.; Kozhukhova, E.A.; Pearton, S.J.; Ren, F.; Lui, L.; Johnson, J.W.; Kargin, N.I.; Ryzhuk, R.V. Deep Centers and Persistent Photocapacitance in AlGaN/GaN High Electron Mobility Transistor Structures Grown on Si Substrates. *J. Vac. Sci. Technol. B Nanotechnol. Microelectron. Mater. Process. Meas. Phenom.* **2013**, *31*, 11211. [CrossRef]
18. Polyakov, A.Y.; Smirnov, N.B.; Ha, M.-W.; Hahn, C.-K.; Kozhukhova, E.A.; Govorkov, A.V.; Ryzhuk, R.V.; Kargin, N.I.; Cho, H.-S.; Lee, I.-H. Effects of Annealing in Oxygen on Electrical Properties of AlGaN/GaN Heterostructures Grown on Si. *J. Alloy. Compd.* **2013**, *575*, 17–23. [CrossRef]
19. Ferrandis, P.; Charles, M.; Gillot, C.; Escoffier, R.; Morvan, E.; Torres, A.; Reimbold, G. Effects of Negative Bias Stress on Trapping Properties of AlGaN/GaN Schottky Barrier Diodes. *Microelectron. Eng.* **2017**, *178*, 158–163. [CrossRef]
20. Ferrandis, P.; El-Khatib, M.; Jaud, M.-A.; Morvan, E.; Charles, M.; Guillot, G.; Bremond, G. Study of Deep Traps in AlGaN/GaN High-Electron Mobility Transistors by Electrical Characterization and Simulation. *J. Appl. Phys.* **2019**, *125*, 35702. [CrossRef]

21. Ferrandis, P.; Charles, M.; Veillerot, M.; Gillot, C. Analysis of Hole-like Traps in Deep Level Transient Spectroscopy Spectra of AlGaN/GaN Heterojunctions. *J. Phys. D Appl. Phys.* **2020**, *53*, 185105. [CrossRef]
22. Lorin, T.; Vandendaele, W.; Gwoziecki, R.; Baines, Y.; Biscarrat, J.; Jaud, M.-A.; Gillot, C.; Charles, M.; Plissonnier, M.; Ghibaudo, G.; et al. On the Understanding of Cathode Related Trapping Effects in GaN-on-Si Schottky Diodes. *IEEE J. Electron Devices Soc.* **2018**, *6*, 956–964. [CrossRef]
23. Sze, S.M.; Ng, K.K. *Physics of Semiconductor Devices*, 3rd ed.; Wiley-Interscience: Hoboken, NJ, USA, 2007; ISBN 978-0-471-14323-9.
24. *FT-1030 DLTFS*; PhysTech GmbH: Moosburg, Germany, 2014.
25. Zhang, T. Deep Levels Characterizations in SiC to Optimize High Voltage Devices. Ph.D. Thesis, Université de Lyon, Lyon, France, 2018.
26. Weiss, S.; Kassing, R. Deep Level Transient Fourier Spectroscopy (DLTFS)—A Technique for the Analysis of Deep Level Properties. *Solid-State Electron.* **1988**, *31*, 1733–1742. [CrossRef]
27. Kindl, D.; Hubík, P.; Krištofik, J.; Mareš, J.J.; Výborný, Z.; Leys, M.R.; Boeykens, S. Deep Defects in GaN/AlGaN/SiC Heterostructures. *J. Appl. Phys.* **2009**, *105*, 93706. [CrossRef]
28. Vurgaftman, I.; Meyer, J.R.; Ram-Mohan, L.R. Band Parameters for III–V Compound Semiconductors and Their Alloys. *J. Appl. Phys.* **2001**, *89*, 5815–5875. [CrossRef]
29. Provencher Algorithm; Automatic Software Packages. 2016. Available online: http://www.s-provencher.com/ (accessed on 29 December 2022).
30. Provencher, S.W. CONTIN: A General Purpose Constrained Regularization Program for Inverting Noisy Linear Algebraic and Integral Equations. *Comput. Phys. Commun.* **1982**, *27*, 229–242. [CrossRef]
31. Wosiński, T. Evidence for the Electron Traps at Dislocations in GaAs Crystals. *J. Appl. Phys.* **1989**, *65*, 6. [CrossRef]
32. Yastrubchak, O.; Wosiński, T.; Mąkosa, A.; Figielski, T.; Porowski, S.; Grzegory, I.; Czernecki, R.; Perlin, P. Capture Kinetics at Deep-Level Electron Traps in GaN-Based Laser Diode. *Phys. Status Solidi C* **2007**, *4*, 2878–2882. [CrossRef]
33. Soh, C.B.; Chua, S.J.; Lim, H.F.; Chi, D.Z.; Liu, W.; Tripathy, S. Identification of Deep Levels in GaN Associated with Dislocations. *J. Phys. Condens. Matter* **2004**, *16*, 6305–6315. [CrossRef]
34. Polenta, L.; Castaldini, A.; Cavallini, A. Defect Characterization in GaN: Possible Influence of Dislocations in the Yellow-Band Features. *J. Appl. Phys.* **2007**, *102*, 63702. [CrossRef]
35. Cho, H.K.; Kim, C.S.; Hong, C.-H. Electron Capture Behaviors of Deep Level Traps in Unintentionally Doped and Intentionally Doped n -Type GaN. *J. Appl. Phys.* **2003**, *94*, 1485–1489. [CrossRef]
36. Cho, H.K.; Kim, K.S.; Hong, C.-H.; Lee, H.J. Electron Traps and Growth Rate of Buffer Layers in Unintentionally Doped GaN. *J. Cryst. Growth* **2001**, *223*, 38–42. [CrossRef]
37. Hacke, P.; Detchprohm, T.; Hiramatsu, K.; Sawaki, N.; Tadatomo, K.; Miyake, K. Analysis of Deep Levels in N-type GaN by Transient Capacitance Methods. *J. Appl. Phys.* **1994**, *76*, 304–309. [CrossRef]
38. Umana-Membreno, G.A.; Parish, G.; Fichtenbaum, N.; Keller, S.; Mishra, U.K.; Nener, B.D. Electrically Active Defects in GaN Layers Grown With and Without Fe-Doped Buffers by Metal-Organic Chemical Vapor Deposition. *J. Electron. Mater.* **2008**, *37*, 569–572. [CrossRef]
39. Duc, T.T.; Pozina, G.; Janzén, E.; Hemmingsson, C. Investigation of Deep Levels in Bulk GaN Material Grown by Halide Vapor Phase Epitaxy. *J. Appl. Phys.* **2013**, *114*, 153702. [CrossRef]
40. Boturchuk, I.; Scheffler, L.; Larsen, A.N.; Julsgaard, B. Evolution of Electrically Active Defects in N-GaN During Heat Treatment Typical for Ohmic Contact Formation. *Phys. Status Solidi A* **2018**, *215*, 1700516. [CrossRef]
41. Chung, H.M.; Chuang, W.C.; Pan, Y.C.; Tsai, C.C.; Lee, M.C.; Chen, W.H.; Chen, W.K.; Chiang, C.I.; Lin, C.H.; Chang, H. Electrical Characterization of Isoelectronic In-Doping Effects in GaN Films Grown by Metalorganic Vapor Phase Epitaxy. *Appl. Phys. Lett.* **2000**, *76*, 897–899. [CrossRef]
42. Honda, U.; Yamada, Y.; Tokuda, Y.; Shiojima, K. Deep Levels in N-GaN Doped with Carbon Studied by Deep Level and Minority Carrier Transient Spectroscopies. *Jpn. J. Appl. Phys.* **2012**, *51*, 04DF04. [CrossRef]
43. Chen, S.; Honda, U.; Shibata, T.; Matsumura, T.; Tokuda, Y.; Ishikawa, K.; Hori, M.; Ueda, H.; Uesugi, T.; Kachi, T. As-Grown Deep-Level Defects in n-GaN Grown by Metal–Organic Chemical Vapor Deposition on Freestanding GaN. *J. Appl. Phys.* **2012**, *112*, 53513. [CrossRef]
44. DeLucca, J.M.; Mohney, S.E.; Auret, F.D.; Goodman, S.A. Pt Schottky Contacts to N-GaN Formed by Electrodeposition and Physical Vapor Deposition. *J. Appl. Phys.* **2000**, *88*, 2593–2600. [CrossRef]
45. Auret, F.D.; Goodman, S.A.; Koschnick, F.K.; Spaeth, J.-M.; Beaumont, B.; Gibart, P. Proton Bombardment-Induced Electron Traps in Epitaxially Grown n-GaN. *Appl. Phys. Lett.* **1999**, *74*, 407–409. [CrossRef]
46. Lee, I.-H.; Polyakov, A.Y.; Smirnov, N.B.; Govorkov, A.V.; Kozhukhova, E.A.; Kolin, N.G.; Boiko, V.M.; Korulin, A.V.; Pearton, S.J. Deep Electron and Hole Traps in Neutron Transmutation Doped N-GaN. *J. Vac. Sci. Technol. B Nanotechnol. Microelectron. Mater. Process. Meas. Phenom.* **2011**, *29*, 41201. [CrossRef]
47. Ito, T.; Nomura, Y.; Selvaraj, S.L.; Egawa, T. Comparison of Electrical Properties in GaN Grown on Si(111) and c-Sapphire Substrate by MOVPE. *J. Cryst. Growth* **2008**, *310*, 4896–4899. [CrossRef]
48. Fang, Z.-Q.; Look, D.C.; Polenta, L. Dislocation-Related Electron Capture Behaviour of Traps in n-Type GaN. *J. Phys. Condens. Matter* **2002**, *14*, 13061–13068. [CrossRef]

49. Lee, I.-H.; Polyakov, A.Y.; Smirnov, N.B.; Hahn, C.-K.; Pearton, S.J. Spatial Location of the Ec-0.6 EV Electron Trap in AlGaN/GaN Heterojunctions. *J. Vac. Sci. Technol. B Nanotechnol. Microelectron. Mater. Process. Meas. Phenom.* **2014**, *32*, 50602. [CrossRef]
50. Polyakov, A.Y.; Smirnov, N.B.; Govorkov, A.V.; Mil, M.G.; Pearton, S.J.; Usikov, A.S.; Shmidt, N.M.; Osinsky, A.V.; Lundin, W.V.; Zavarin, E.E.; et al. Deep Levels Studies of AlGaN/GaN Superlattices. *Solid-State Electron.* **2003**, *47*, 671–676. [CrossRef]
51. Lee, W.I.; Huang, T.C.; Guo, J.D.; Feng, M.S. Effects of Column III Alkyl Sources on Deep Levels in GaN Grown by Organometallic Vapor Phase Epitaxy. *Appl. Phys. Lett.* **1995**, *67*, 1721–1723. [CrossRef]
52. Fang, Z.-Q.; Look, D.C.; Kim, W.; Morkoç, H. Characteristics of Deep Centers Observed in N-GaN Grown by Reactive Molecular Beam Epitaxy. *MRS Online Proc. Libr. (OPL)* **1999**, *595*, 6. [CrossRef]
53. Jenkins, D.W.; Dow, J.D. Electronic Structures and Doping of InN, InxGa1−xN, and InxAl1−xN. *Phys. Rev. B* **1989**, *39*, 3317–3329. [CrossRef] [PubMed]
54. Gorczyca, I.; Svane, A.; Christensen, N.E. Theory of Point Defects in GaN, AlN, and BN: Relaxation and Pressure Effects. *Phys. Rev. B* **1999**, *60*, 8147–8157. [CrossRef]
55. Matsubara, M.; Bellotti, E. A First-Principles Study of Carbon-Related Energy Levels in GaN. I. Complexes Formed by Substitutional/Interstitial Carbons and Gallium/Nitrogen Vacancies. *J. Appl. Phys.* **2017**, *121*, 195701. [CrossRef]
56. Zhong, J.; Yao, Y.; Zheng, Y.; Yang, F.; Ni, Y.-Q.; He, Z.-Y.; Shen, Z.; Zhou, G.-L.; Zhou, D.-Q.; Wu, Z.-S.; et al. Influence of Dry-Etching Damage on the Electrical Properties of an AlGaN/GaN Schottky Barrier Diode with Recessed Anode. *Chin. Phys. B* **2015**, *24*, 97303. [CrossRef]
57. Tanaka, T.; Shiojima, K.; Mishima, T.; Tokuda, Y. Deep-Level Transient Spectroscopy of Low-Free-Carrier-Concentration n-GaN Layers Grown on Freestanding GaN Substrates: Dependence on Carbon Compensation Ratio. *Jpn. J. Appl. Phys.* **2016**, *55*, 61101. [CrossRef]
58. Arehart, A.R.; Corrion, A.; Poblenz, C.; Speck, J.S.; Mishra, U.K.; Ringel, S.A. Deep Level Optical and Thermal Spectroscopy of Traps in N-GaN Grown by Ammonia Molecular Beam Epitaxy. *Appl. Phys. Lett.* **2008**, *93*, 112101. [CrossRef]
59. Polyakov, A.Y.; Smirnov, N.B.; Kozhukhova, E.A. Temperature Stability of High-Resistivity GaN Buffer Layers Grown by Metalorganic Chemical Vapor Deposition. *J. Vac. Sci. Technol. B* **2013**, *31*, 8. [CrossRef]
60. Götz, W.; Johnson, N.M.; Amano, H.; Akasaki, I. Deep Level Defects in N-type GaN. *Appl. Phys. Lett.* **1994**, *65*, 463–465. [CrossRef]
61. Haase, D.; Schmid, M.; Kürner, W.; Dörnen, A.; Härle, V.; Scholz, F.; Burkard, M.; Schweizer, H. Deep-level Defects and N-type-carrier Concentration in Nitrogen Implanted GaN. *Appl. Phys. Lett.* **1996**, *69*, 2525–2527. [CrossRef]